CHIN. PHYS. LETT. Vol. 38, No. 7 (2021) 076102

Improvement of Cyclic Stability of $Na_{0.67}Mn_{0.8}Ni_{0.1}Co_{0.1}O_2$ via Suppressing Lattice Variation

Zhongmin Ren(任重民)[1], Muqin Wang(王木钦)[1,3*], Shuaishuai Chen(陈帅帅)[2], Lei Ding(丁雷)[2], Hua Li(李华)[1], Jian Liu(刘健)[1], Jieyun Zheng(郑杰允)[4*], Zhihong Liu(刘志宏)[1], Deyu Wang(王德宇)[1,2*], and Mingkui Wang(王鸣魁)[3]

[1]*Key Laboratory of Optoelectronic Chemical Materials and Devices, School of Chemical and Environmental Engineering, Jianghan University, Wuhan 430056, China*
[2]*Ningbo Institute of Materials Technology and Engineering, Chinese Academy of Sciences, Ningbo 315201, China*
[3]*Wuhan National Laboratory for Optoelectronics, Huazhong University of Science & Technology, Wuhan 430074, China*
[4]*Institute of Physics, Chinese Academy of Sciences, Beijing 100190, China*

(Received 8 March 2021; accepted 10 May 2021; published online 3 July 2021)

Strategies to prolong operational life are highly pursued to strengthen the advantage of cost-effectiveness on sodium-ion batteries (SIBs). We demonstrate the crucial influence of particles' internal mechanical strains on durability of cathode, which does not attract enough attentions from the community. Among the investigated samples, 2% Ti-modified-$Na_{0.67}Ni_{0.1}Co_{0.1}Mn_{0.8}O_2$ suppresses the *c*-axis lattice variation by 38%, attains the reversible capacity 86% higher after 200 cycles, and still keeps intact morphology. This approach indicates that the mechanical properties could tailor cyclic stability of cathode, which is particular important to further improve competitiveness for SIBs.

DOI: 10.1088/0256-307X/38/7/076102

Energy storage technologies have been seriously developed to fulfill the ever-increasing requirements of our modern daily life. Lithium ion batteries (LIBs) were the most successful technologies proposed in recent decades to provide sustainable energy.[1,2] They have dominated the market of consumer electronics & electric vehicles and penetrated into the utilization of smart grids. However, the shortage of the lithium resource limited its potential large-scale application, such as energy-storage batteries for new-energy plants where harvested energy from solar and wind.[3–5] Therefore various alternatives were developed to replace lithium ion batteries for the security of resources.

Sodium-ion batteries (SIBs) were the most promising alternative, especially in large-scale utilizations, owing to the rich abundance of sodium.[6–8] Series of cathode materials with less amount of precious metal elements were developed to further lower material cost of SIBs, such as $Na_{0.67}Ni_{0.1}Fe_{0.1}Mn_{0.8}O_2$ and $Na_{0.5}Ni_{0.1}Co_{0.15}Mn_{0.65}Mg_{0.1}O_2$. Also the manufactory advised the equipment of LIBs, which further reduced the cost of this new technology. Therefore, although they were proposed in recent years, SIBs presented the excellent competitiveness on the balance of cost and performance. Even some pioneering enterprises claimed their products to have possessed the behavior close to lithium ion batteries with the cost close to lead-acid batteries.

The long cyclic life was highly pursued for sodium ion batteries to further strengthen the advantage of cost-effectiveness. However, their durability was hindered by various drawbacks. In cathode side, cation mixing, interface sensitivity and side reactions between the charge-state electrode and electrolytes were the key reasons for cell degradation.[9–18] Some effective strategies have been adopted to prolong their cyclic life. For instance, calcination procedures and cationic substitutions were optimized to restrain the cation disorder of P2-layered structure cathodes.[19–21] Concentration gradient and core-shell structures have also been applied to reduce side reactions of Na-NCM cathode materials with electrolyte by the stable surface/interface.[22,23]

Besides the aforementioned factors, we highly hypothesized that mechanical characteristics should play a crucial role on the cyclic stability of active materials utilized in sodium ion batteries. It took place in LIBs where durability was seriously deteriorated by particle cracking and then electrolyte dry-up.[24–26] From our previous works, the mechanical stress could be roughly estimated by the change of lattice *c* with Hooke's law and the whole process could be understood with the fatigue-fractured model.[27–30] The influence of mechanical stress should be more serious for SIB cathodes for Na^+ ionic radius is 0.97 Å, ∼30% larger than Li^+ ionic radius.[31–37] However, little attention was paid to this topic.

In this work, we demonstrate the influence of mechanical stress on durability of cathodes for SIBs

Supported by the China Postdoctoral Science Foundation (Grant No. 2020M682391), Beijing Municipal Science and Technology Commission (Grant No. Z191100004719001), the Start-Up Funding of Jianghan University, and the "Chutian Scholar Program" of Hubei Province.
*Corresponding authors. Email: mokinwong@163.com; jyzheng@iphy.ac.cn; wangdeyu@jhun.edu.cn
© 2021 Chinese Physical Society and IOP Publishing Ltd

with P2-$Na_{0.67}Ni_{0.1}Co_{0.1}Mn_{0.8}O_2$. According to the structural characteristics, the 2%-Ti modification seriously suppresses the variation of c axis from 0.127 Å to 0.079 Å, ∼38% less than the pristine, and attains the highest capacity retention ratio, still attaining 91.2 mA·h·g^{-1} after 200 cycles, much higher than the pristine sample (49.0 mA·h·g^{-1}). Postmortem analysis proves the optimal sample keeps the intact morphology, instead of the pulverized particles for other materials (Fig. 1). Our approaches illustrate the important effect of mechanical characteristics on durability of SIBs.

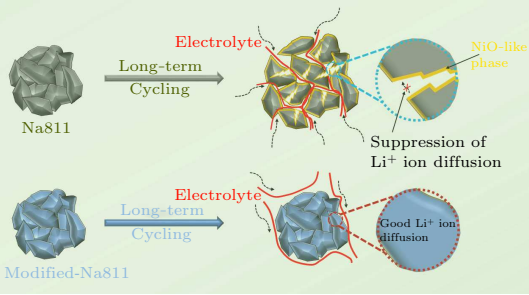

Fig. 1. The schematic illustration of degradation and modification for Na811.

Experimental Section—Materials. The layered P2-$Na_{0.67}Ni_{0.1}Co_{0.1}Mn_{0.8}O_2$ (Na811) was synthesized through a solid state reaction method from stoichiometric values of Na_2CO_3 (AR, 99.5%), $Ni(CH_3COO)_2{\cdot}4H_2O$ (AR, 99.0%), $Co(CH_3COO)_2{\cdot}4H_2O$ (AR, 99.0%) and $Mn(CH_3COO)_2{\cdot}4H_2O$(AR, 99.0%). P2-$Na_{0.67}Ni_{0.1-x}Co_{0.1}Mn_{0.8}Ti_xO_2$ (x = 0.02, 0.05) were also synthesized via the same method with different amounts of TiO_2. The above mixtures were sintered at 950 ℃ for 12 h under pure oxygen. Then the furnace was cooled down to room temperature to obtain the samples, which were stored in an argon-filled glove box until use.

Coin Cells Assembly. A homogenous slurry, consisting of 80 wt% active cathode materials, 10 wt% super P and 10 wt% polyvinylidene fluoride (PVDF) binder, was prepared by dispersing the solid powders in N-methyl pyrrolidone (NMP) solvent. After stirring for 4 h, the as-prepared slurry was coated on aluminum (Al) foil. The cathode-coated Al foil was dried at 120 ℃ under vacuum and punched into ϕ14 mm disks. CR2032 coin-cells were assembled using the cathode-coated Al foil as cathode, Na metal as anode, glass fiber as separator and 1.0 M $NaClO_4$ dissolved in propylene carbonate (EC) with 5% fluoroethylene carbonate (FEC) in volume as electrolyte, respectively. The coin-cells were assembled in the argon-filled glove box, where H_2O and O_2 content was controlled less than 1 ppm.

Characterization. The crystalline structure of as-prepared powders was characterized by x-ray diffraction (Bruker AXS, D8 Advance x-ray diffractometer), equipped with Cu K_α radiations ($\lambda = 1.5406$ Å). The XRD patterns were recorded in the 2θ range of 10° and 90° with a scan rate of 0.02° per second.

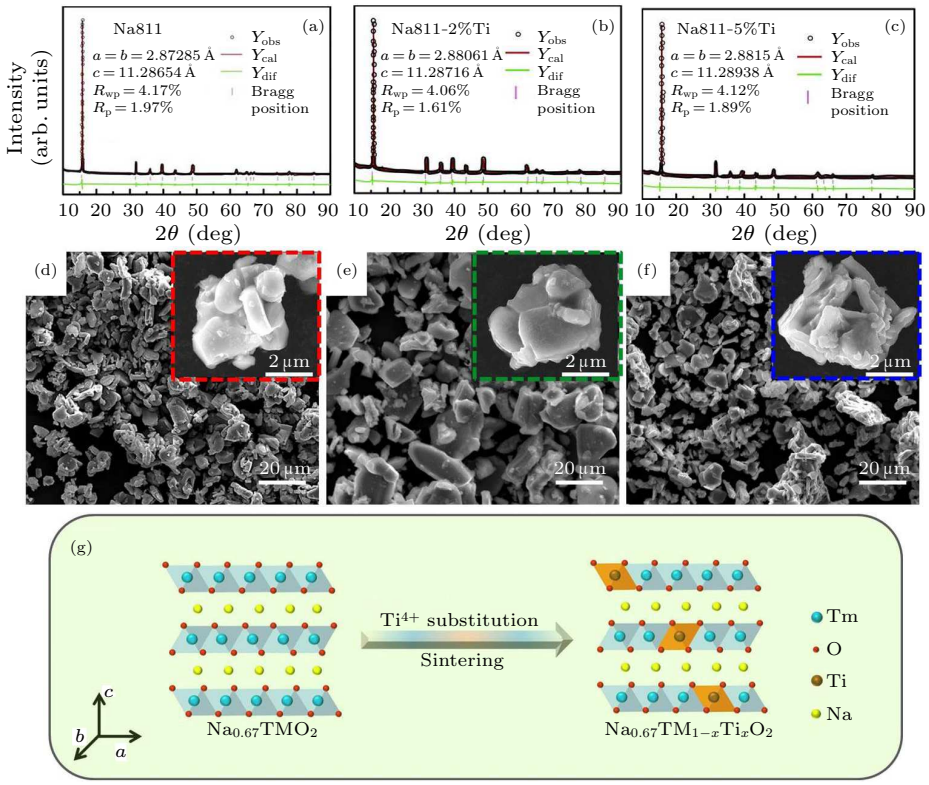

Fig. 2. X-ray diffraction (XRD) pattern and Rietveld plots of the samples: (a) Na811, (b) Na811-2%Ti, (c) Na811-5%Ti. Scanning electron microscopy (SEM) images of the samples: (d) Na811, (e) Na811-2%Ti, (f) Na811-5%Ti. (g) Structural change of Na811 with Ti doped. R_{wp} and R_p are the factors to evaluate the precision of refinement. R_{wp}: weighted profile R-factor; R_p: profile residual (unweighted).

The as-obtained XRD patterns were refined by the Rietveld method using the GASA/EXPGUI program. The *in situ* XRD patterns (2θ = 10°—70°, Cu K_α radiations, 30 min per scan) were obtained using a D8 Advanced x-ray diffractometer. The coin cells for *in situ* measurements were assembled using a beryllium window, which has been used as the cathode current collector and coated with as-prepared cathodes. The morphological analysis was carried out using scanning electron microscopy (SEM, FEI, QUANTA 250 FEG) and transmission electron microscopy (TEM, Talos F200, 200 kV). The particle cutting was prepared by focused ion beam (FIB, SCIOS, FEI). The DSC curves were measured between room temperature and 300 ℃ at a scan rate of 5 ℃/min.

Electrochemical Measurements. The galvanostatic charge-discharge measurements were performed by battery testers (Land 2001A, Wuhan, China) in the voltage range of 1.5–4.3 V vs Na/Na^+ at 25 ℃ under different current densities. After charging to 4.3 V vs Na/Na^+, the electrochemical impedance spectroscopy (EIS) of the coin-cells was carried out in the frequency range from 0.1 MHz to 0.1Hz by CHI600D electrochemical workstation. The cyclic voltammetry (CV) was carried out in the voltage range of 1.5–4.9 V vs Na/Na^+ at the scan rate of 0.1 mV/s.

Results and Discussion. The structures and morphologies of the pristine and Ti-modified P2-$Na_{0.67}Mn_{0.8}Ni_{0.1}Co_{0.1}O_2$ (Na811, Na811-2%Ti & Na811-5%Ti) were shown in Fig. 2. The final products kept a layered structure with $P63/mmc$ space group without impurity phases, indicating Ti element entered into the crystalline lattice. The particles of synthetic samples were averaged at ∼2 μm and titanium element was evenly distributed in the particles as shown in Fig. S1 (Supplementary Information). According to the refined results, Ti(Ⅳ) should take the positions of transitional metal ions, as shown in Tables S1–S3. According to our previous work,[37] the lattice variation should be lessened after Ti-substitution.

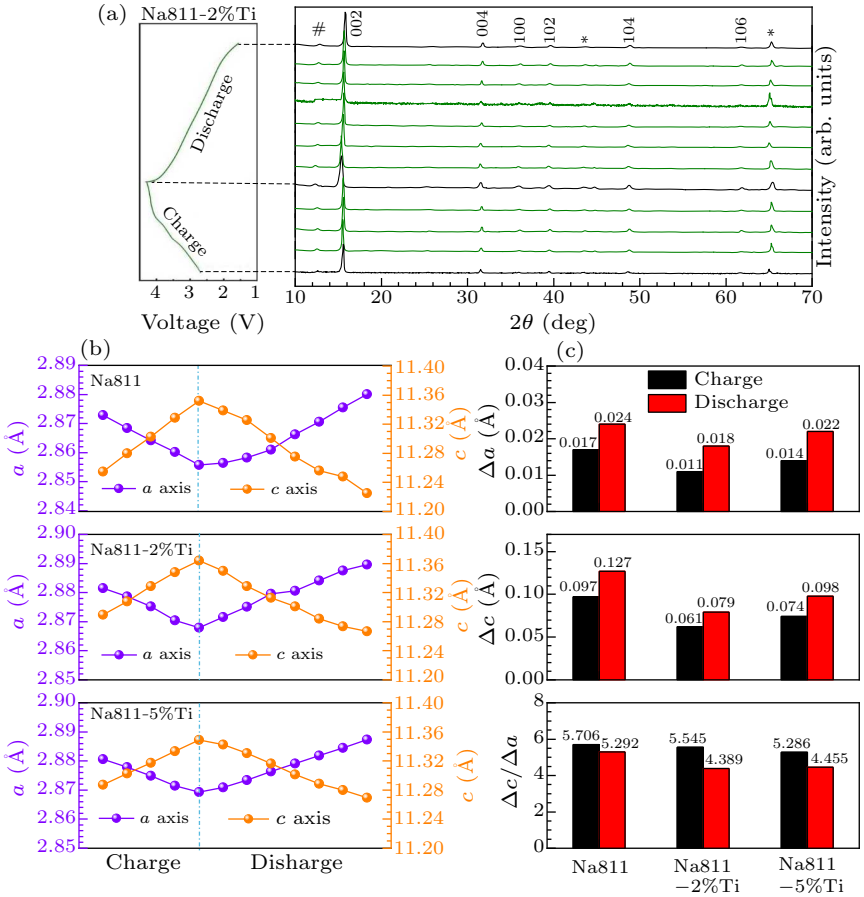

Fig. 3. (a) *In situ* XRD characterization of Na811-2%Ti; (b) variation of lattice c on all investigated samples during 1st charge and discharge; (c) Δa and Δc of all investigated during charge and discharge.

The structure evolution of Na811 was traced via *in situ* XRD analysis. The cells were operated between 1.5 V and 4.3 V vs Na/Na^+ with a current density of 40 $mA{\cdot}g^{-1}$ (0.2 C). During charge, the (002) and (004) peaks of the P2 phase slightly moved toward to a lower angle, while the (100) peak shifted to higher angle. At the end of charge, no extra peaks beyond P2 phase are discovered, as shown in Fig. S2. The patterns of *in situ* XRD for Na811-2%Ti & Na811-5%Ti were similar to the pristine sample [Fig. 3(a) and Fig. S2]. This shows that Ti substitution did not change the cathode's structure and its evolution during cycling, which was consistent with other cathodes.[36,38,39]

In contrast, Ti-modification obviously changed

the lattice variation of P2-$Na_{0.67}Mn_{0.8}Ni_{0.1}Co_{0.1}O_2$. Based on the *in situ* XRD results, the a-axis of Na811-2% was monotonically shrunk from 2.882 Å to 2.871 Å during charge, and gradually elongated to 2.889 Å when discharged to the end [Fig. 3(b)]. In contrast, the c-axis was firstly elongated to 11.35 Å and then shrunk to 11.27 Å during delithiation and lithiation process, as shown in Fig. 3(b). The variations of a-axis (Δa) and c-axis (Δc) for Na811-2%Ti were 0.018 Å & 0.079 Å for discharge, ∼24% and ∼ 38% less than the pristine sample [Fig. 3(c)], which is similar to our previous results in cathode of LIBs.[37] As for Na811-5% Ti, the variation of lattice parameters does not change too much, in which the a-axis shrunk to 2.868 Å, then gradually elongated to 2.890 Å and the c-axis elongated to 11.36 Å and then shrunk to 11.27 Å during in-cycling. It may be that redundant Ti replaces the octahedral coordinated transition metal, which cannot effectively reduce the electrostatic force between the transition metal element and the oxygen layer (Fig. S3).[40]

According to our experience, the mechanical strain could be considered as elastic deformation and roughly estimated by Hooke's law. The mechanical strain of cathode particles should be proportional to the mechanical stress, namely the dominant variation of lattice axis. In P2-type cathodes, since Δc is ∼5 times of the Δa [Fig. 3(c)], the anisotropic change of c-axis could be used to roughly estimate the internal mechanical stress.[41–46] Based on our understanding,[36,37] the cathode particles were gradually lacerated by the internal stress via the fatigue-fracture model.

$$F_n = Y\sigma_n a_n^{1/2}, \tag{1}$$

$$F_n = F_0(1-D_1)(1-D_2)(1-D_3)\cdots(1-D_n), \tag{2}$$

where F_n, σ_n and a_n represent the fracture strength, internal stress and micro-crack length on the surface of the particle during the nth cycle, respectively. F_0 denotes the intrinsic fracture strength, whereas D_1, D_2, D_3 and D_n represent the degrees of damage during 1st, 2nd, 3rd and nth cycle.

Meanwhile, the internal stress (σ_n) can be calculated by the difference of c-axis (Δc) and Young moduli of the cathodes (Y). Since the Young moduli of modified samples are approximately the same, the internal stress of the all samples could be compared with Δc. Therefore, 2% Ti-modified sample presented the least internal stress among the investigated samples.

$$\Delta c_{\text{Na811 cycling}} = 1.59\Delta c_{\text{Na}-811-2\%\text{ Ti cycling}} = 1.31\Delta c_{\text{Na}-811-5\%\text{ Ti cycling}}. \tag{3}$$

The electrochemical performances of all the synthesized samples were evaluated between 1.5 ∼ 4.3 V vs Na^+/Na by coin cells with various current densities, as shown in Fig. 4(a). Under 0.1 C (≈ 20 mA·h·g^{-1}), Na811 delivered 160.4 mA·h·g^{-1}, slightly higher than Ti modified samples, 151.6 mA·h·g^{-1} and 139.8 mA·h·g^{-1} for 2% and 5% Ti-Na811, respectively [Figs. 4(b)–4(d)]. However, Na811 underwent a rapid decay with only 49.0 mA·h·g^{-1} at 0.5 C after 200 cycles, while the Na811-2%Ti and Na811-5%Ti could keep 91.2 mA·h·g^{-1} and 61.5 mA·h·g^{-1} under the same condition [Figs. S4(a)–S4(c)]. The capacity retention and the rapid speed of Na811-Ti were about 2 time higher than Na811 [Figs. S4(d) and S4(e)]. Also Ti-modification ameliorated the rate capability of Na-811.

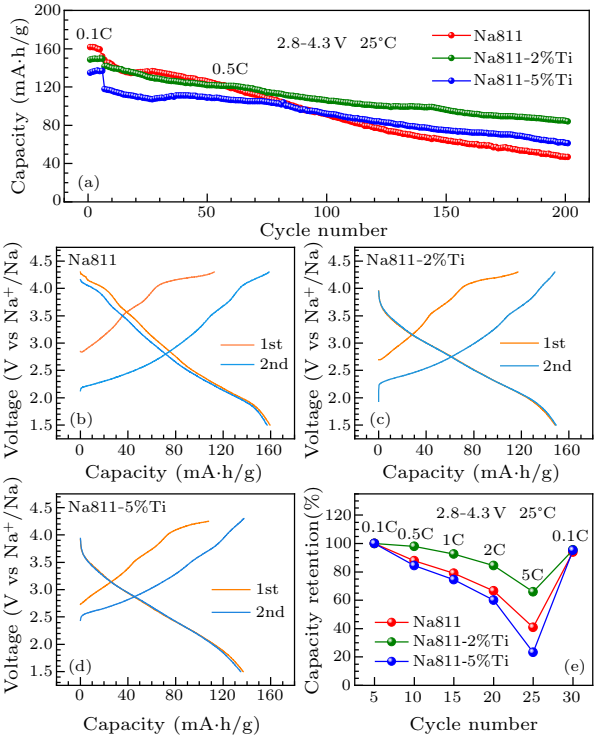

Fig. 4. (a) Cyclic performance of Na811, Na811-2%Ti and Na811-5%Ti. Charge and discharge profiles at selected cycles at 0.1 C (1st and 2nd): (b) Na811, (c) Na811-2%Ti, (d) Na811-5%Ti. (e) Rate retention of Na811, Na811-2%Ti and Na811-5%Ti.

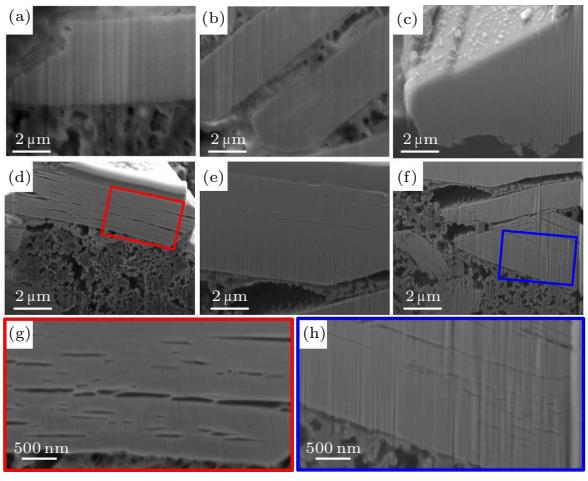

Fig. 5. Cross-sectional SEM of the samples before cycling: (a) Na811, (b) Na811-2%Ti, (c) Na811-5%Ti. Cross-sectional SEM of the samples after 200 charge/discharge cycles, measured at the current rate of 0.5 C: [(d), (g)] Na811, (e) Na811-2%Ti, [(f), (h)] Na811-5%Ti.

To verify the effect of internal stress on cathode damage, the particles of Na811, Na811-2%Ti and Na811-5%Ti in initial state and the 200th cycle were compared via the cross-sectional SEM images, as shown in Figs. 5(a)–5(f). The samples before cycling possessed the smooth surface without any cracks, indicating the bulky entireness. After durability test, the Na811-2%Ti kept the intact morphology of the particles without any obvious cracks [Fig. 5(e)]. In contrast, Na811 particles showed severely cleavages with the cracks about 50–250 nm, as shown in Fig. 5(g), which seemed like layer separation via the cleavage plane. As for 5%-Ti modified sample, obvious cracks were also observable in the selected regions [Fig. 5(h)]. The sequence of bulky entireness for the samples was the same as that of their capacity retention ratio, proving the crucial effect of mechanical damage on cyclic stability of cathode.

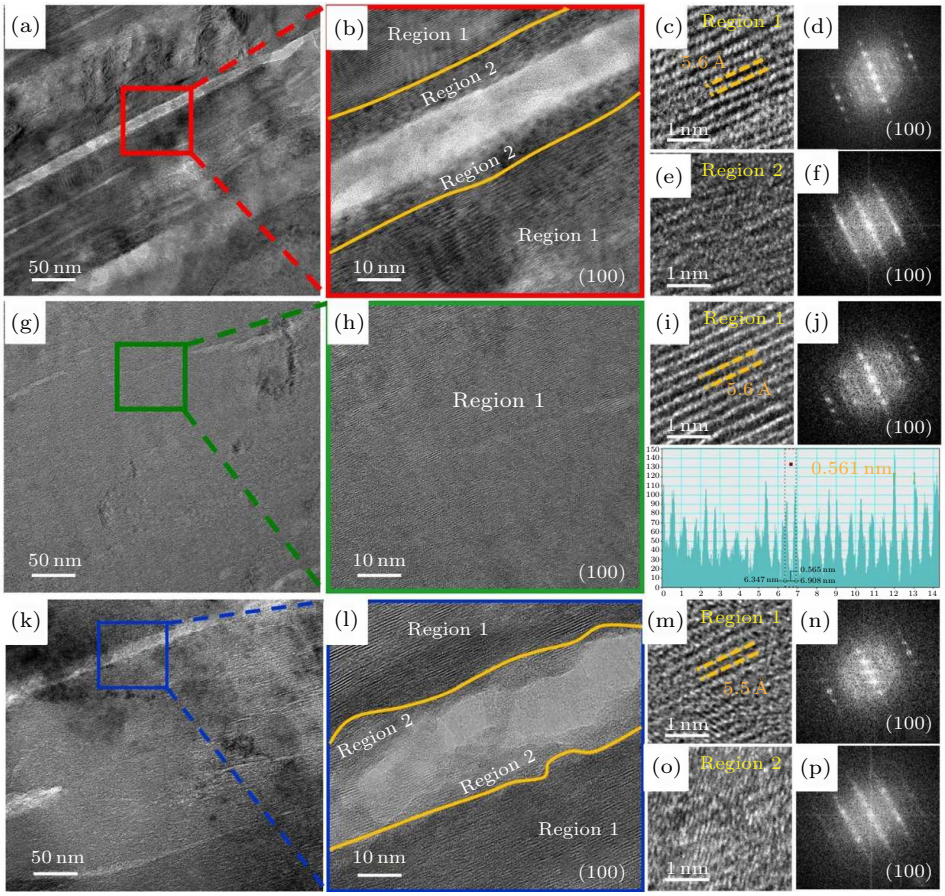

Fig. 6. [(a), (b), (c), (e), (g), (h), (i) & (k), (l), (m), (n)] TEM images of Na811, Na811-2%Ti & Na811-5%Ti cathodes after 200 charge/discharge cycles, measured at the current rates of 0.5 C. [(d), (f), (j) & (n), (p)] The corresponding FFT images of [(c), (e), (i) & (m), (o)].

High-resolution TEM analysis was used to test the structure fracture on the particles during cycling. As shown in Figs. S5(a) and S5(b) in the Supplementary Information, the line dislocations of Na811 and Na811-5%Ti were observed in (100) plane after 100 cycles. They indicate that the minor damage of the bulk particle was gradually formed before fracture, which was reported in previous works.[31,32] The ultrathin cross sections of particles for all samples after 200 cycles [Figs. 6(a)–6(p)] were observed to reveal the microstructural changes. In the case of Na811 [Fig. 6(a)], the serious structure fracture was discovered, and the micro-cracks permeated the entire cross section. From the magnification [Figs. 6(b)–6(d)], region I, ∼7 nm to the boundary kept the layered structure with lattice spacing of 5.6 Å. Region Ⅱ shows a NiO-like rock-salt phase on the surface, which was firstly proposed by Ryn *et al.*[47] It probably generated due to the side reactions between the new interface and electrolyte [Figs. 6(e)–6(f)]. The Na811-5% Ti also exhibited the similar phase transition near the edge of the micro-cracks in Figs. 6(k)–6(p). In contrast, no impurity phase was observed for Na811-2% Ti, indicating that no electrolytes permeated into the particles [Figs. 6(g)–6(j)].

Cyclic voltammetry (CV) measurements were firstly used to analyze the as-prepared cathode samples [Figs. S6(a)–S6(c)]. All the three samples possessed three redox couples at 2.51 V, 3.75 V and 4.15 V vs Na^+/Na. After 100/200 cycles, the CV curves for Na811-2%Ti were almost overlapped with the 1st cycle, whereas Na811 and Na811-5%Ti gradually devi-

ated from the initial (Fig. S6). Furthermore, the results of electrochemical impedance spectroscopy (EIS) and open circuit potential showed that the overpotential of the 2% Ti doped sample (Na811-2%Ti) was not obviously enhanced after 200 cycles, whereas the other samples seriously aggrandized after durability test, as shown in Figs. S6(d)–S6(e) and Figs. S7(a)–S7(f). The results of pulverized particles, new NiO-like phase and augmented polarizations for Na811 and Na811-5%Ti further proved that the mechanical-induced cracked particles were reacted with electrolyte to augment the polarization and deteriorate the durability. Namely, mechanical tolerance of SIB cathodes exerted a crucial effect on their cyclic stability.

In summary, we have demonstrated the influence of mechanical damages on cyclic performance of P2-$Na_{0.67}Mn_{0.8}Ni_{0.1}Co_{0.1}O_2$ (Na811). Ti modification with appropriate amount could suppress the lattice variation, namely the internal mechanical stress, during Na^+ insertion and extraction. As a result, the 2%Ti-modified-Na811 attains a reversible capacity of $91.2\,mA{\cdot}h{\cdot}g^{-1}$ at 0.5 C after 200 cycles, which is ∼1.86 times of Na811. The present study demonstrates that the durability of SIB cathodes is tailored by mechanical characteristics of particles, which are able to further lower the operational cost of sodium ion batteries.

References

[1] Yabuuchi N, Kubota K, Dahbi M and Komaba S 2014 *Chem. Rev.* **114** 11636
[2] Kundu D, Talaie E, Duffort V and Nazar L F 2015 *Angew. Chem. Int. Ed.* **54** 3431
[3] Liu W, Oh P, Liu X, Lee M J, Cho W, Chae S, Kim Y and Cho J 2015 *Angew. Chem. Int. Ed.* **54** 4440
[4] Kim J, Lee H, Cha H, Yoon M, Park M and Cho J 2018 *Adv. Energy Mater.* **8** 1702028
[5] Thackeray M M, Wolverton C and Isaacs E D 2012 *Energy Environ. Sci.* **5** 7854
[6] Li H S, Ding Y, Ha H, Shi Y, Peng L L, Zhang X G, Ellison C J and Yu G H 2017 *Adv. Mater.* **29** 1700898
[7] Wang P F, You Y, Yin Y X, Wang Y S, Wan L J, Gu L and Guo Y G 2016 *Angew. Chem. Int. Ed.* **55** 7445
[8] Yoon H J, Na R K, Jin H J and Yun Y S 2018 *Adv. Energy Mater.* **8** 1870027
[9] Xiong X, Ding D, Bu Y, Wang Z, Huang B, Guo H and Li X 2014 *J. Mater. Chem. A* **2** 11691
[10] Sun Y K, Myung S T, Park B C, Prakash J, Belharouak I and Amine K 2009 *Nat. Mater.* **8** 320
[11] Jung Y S, Lu P, Cavanagh A S, Ban C, Kim G H, Lee S H, George S M, Harris S J and Dillon A C 2013 *Adv. Energy Mater.* **3** 213
[12] Choi N S, Chen Z, Freunberger S A *et al.* 2012 *Angew. Chem. Int. Ed.* **51** 9994
[13] Jung S K, Gwon H, Hong J, Park K Y, Seo D H, Kim H, Hyun J, Yang W and Kang K 2014 *Adv. Energy Mater.* **4** 1300787
[14] Scrosati B and Garche J 2010 *J. Power Sources* **195** 2419
[15] Lee S W, Kim M S, Jeong J H *et al.* 2017 *J. Power Sources* **360** 206
[16] Yoon W S, Hanson J, McBreen J and Yang X Q 2006 *Electrochem. Commun.* **8** 859
[17] Oh P, Song B, Li W and Manthiram A 2016 *J. Mater. Chem. A* **4** 5839
[18] Cho Y, Oh P and Cho J 2013 *Nano Lett.* **13** 1145
[19] Hwang J Y, Kim J, Yu T Y and Sun Y K 2019 *Adv. Energy Mater.* **9** 1803346
[20] Zhang X, Guo S, Liu P, Li Q, Xu S, Liu Y, Jiang K, He P, Chen M, Wang P and Zhou H 2019 *Adv. Energy Mater.* **9** 1900189
[21] Wang Q, Mariyappan S, Vergnet J, Abakumov A M, Rousse G, Rabuel F, Chakir M and Tarascon J M 2019 *Adv. Energy Mater.* **9** 1901785
[22] Zhu Y E, Qi X G, Chen X Q, Zhou X L, Zhang X, Wei J P, Hu Y S and Zhou Z 2016 *J. Mater. Chem. A* **4** 11103
[23] Xu J L, Han Z, Jiang K, Bai P, Liang Y, Zhang X, Wang P, Guo S and Zhou H 2020 *Small* **16** 1904388
[24] Wang K, Wan H, Yan P, Chen X, Fu J, Liu Z, Deng H, Gao F and Sui M 2019 *Adv. Mater.* **31** 1904816
[25] Wang Q C, Meng J K, Yue X Y, Qiu Q Q, Song Y, Wu X J, Fu Z W, Xia Y Y, Shadike Z, Wu J, Yang X Q and Zhou Y N 2019 *J. Am. Chem. Soc.* **141** 840
[26] Zhang K, Kim D, Hu Z, Park M, Noh G, Yang Y, Zhang J, Lau V W, Chou S L, Cho M, Choi S Y and Kang Y M 2019 *Nat. Commun.* **10** 5203
[27] Hu X, Qiang W and Huang B 2017 *Energy Storage Mater.* **8** 141
[28] Cheng X, Liu M, Yin J, Ma C, Dai Y, Wang D, Mi S, Qiang W, Huang B and Chen Y 2020 *Small* **16** 1906433
[29] Ren Z, Zhang X, Liu M, Zhou J, Sun S, He H and Wang D 2019 *J. Power Sources* **416** 104
[30] Ren Z, Shen C, Liu M, Liu J, Zhang S, Yang G, Huai L, Liu X, Wang D and Li H 2020 *Energy Storage Mater.* **28** 1
[31] Wang K, Yan P and Sui M 2018 *Nano Energy* **54** 148
[32] Yan P, Zheng J, Chen T, Luo L, Jiang Y, Wang K, Sui M, Zhang J G, Zhang S and Wang C 2018 *Nat. Commun.* **9** 2437
[33] Yan P, Zheng J, Gu M, Xiao J, Zhang J G and Wang C M 2017 *Nat. Commun.* **8** 14101
[34] Xu Z, Rahman M M, Mu L, Liu Y and Lin F 2018 *J. Mater. Chem. A* **6** 21859
[35] Guo S H, Liu P, Yu H J, Zhu Y B, Chen M W, Ishida M and Zhou H S 2015 *Angew. Chem. Int. Ed.* **54** 5894
[36] Mu L Q, Xu S Y, Li M, Hu Y S, Li H, Chen L Q and Huang X J 2015 *Adv. Mater.* **27** 6928
[37] Singh G, Tapia-Ruiz N, Lopez D A J M, Maitra U, Somerville J W, Armstrong A R, de Martinez I J, Rojo T and Bruce P G 2016 *Chem. Mater.* **28** 5087
[38] Wang P, Xiao Y, Piao N, Wang Q, Ji X, Jin T, Guo Y, Liu S, Deng T, Cui C, Chen L, Guo Y, Yang X and Wang C 2020 *Nano Energy* **69** 104474
[39] Liu K, Tan S, Moon J, Jafta C J, Li C, Kobayashi T, Lyu H, Bridges C A, Men S, Guo W, Sun Y, Zhang J, Paranthaman M P, Sun X and Dai S 2020 *Adv. Energy Mater.* **10** 2000135
[40] Xiao B W, Liu H S, Liu J *et al.* 2017 *Adv. Mater.* **29** 1703764
[41] Yoon C S, Jun D W, Myung S T and Sun Y K 2017 *Acs. Energy Lett.* **2** 1150
[42] Zhou Y N, Wang P F, Niu Y B, Li Q, Yu X, Yin Y X, Xu S and Guo Y G 2019 *Nano Energy* **55** 143
[43] Hwang J Y, Myung S T and Sun Y K 2017 *Chem. Soc. Rev.* **46** 3529
[44] Wang Y S, Yu X Q, Xu S Y, Bai J M, Xiao R J, Hu Y S, Li H, Yang X Q, Chen L Q and Huang X J 2013 *Nat. Commun.* **4** 2365
[45] Yabuuchi N, Kajiyama M, Iwatate J, Nishikawa H, Hitomi S, Okuyama R, Usui R, Yamada Y and Komaba S 2012 *Nat. Mater.* **11** 512
[46] Berthelot R, Carlier D and Delmas C 2011 *Nat. Mater.* **10** 74
[47] Ryn H, Park K, Yoon C and Sun Y 2018 *Chem. Mater.* **30** 1155

Supplementary Information for "Improvement of Cyclic Stability of $Na_{0.67}Mn_{0.8}Ni_{0.1}Co_{0.1}O_2$ via Suppressing Lattice Variation"

Zhongmin Ren(任重民)[1], Muqin Wang(王木钦)[1,3*], Shuaishuai Chen(陈帅帅)[2], Lei Ding(丁雷)[2], Hua Li(李华)[1], Jian Liu(刘健)[1], Jieyun Zheng(郑杰允)[4*], Zhihong Liu(刘志宏)[1], Deyu Wang(王德宇)[1,2]*, Mingkui Wang(王鸣魁)[3c]

1 Key Laboratory of Optoelectronic Chemical Materials and Devices, School of Chemical and Environmental Engineering, Jianghan University, Wuhan 430056, China.

2 Ningbo Institute of Materials Technology and Engineering, Chinese Academy of Sciences, Ningbo 315201, China.

3 Huazhong University of Science & Technology, Wuhan 430074, China

4 Institute of Physics, Chinese Academy of Science, Beijing 10080, China

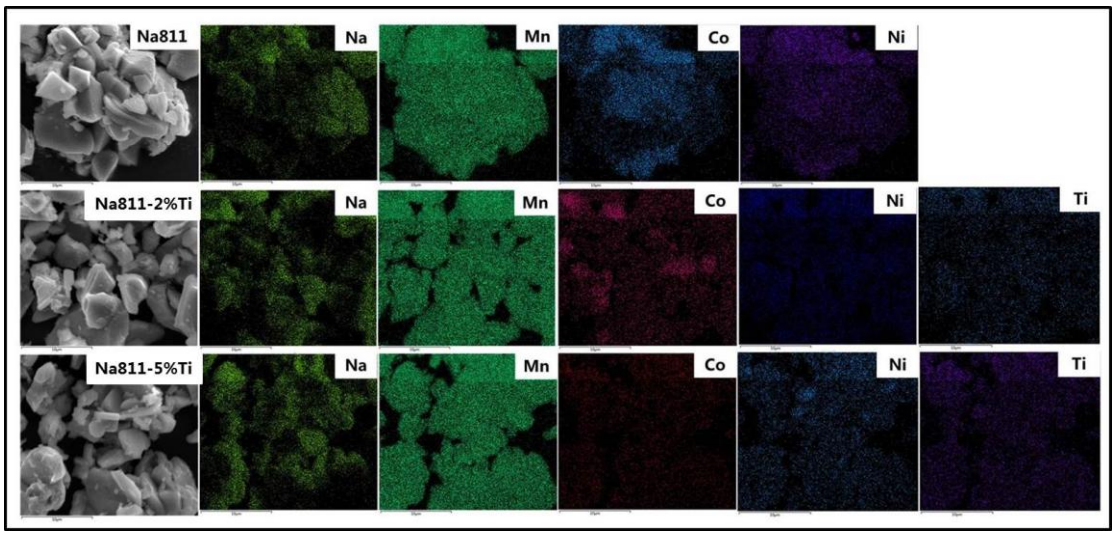

Fig. S1. SEM and EDS images of Na811, Na811-2%Ti, Na811-5%Ti.

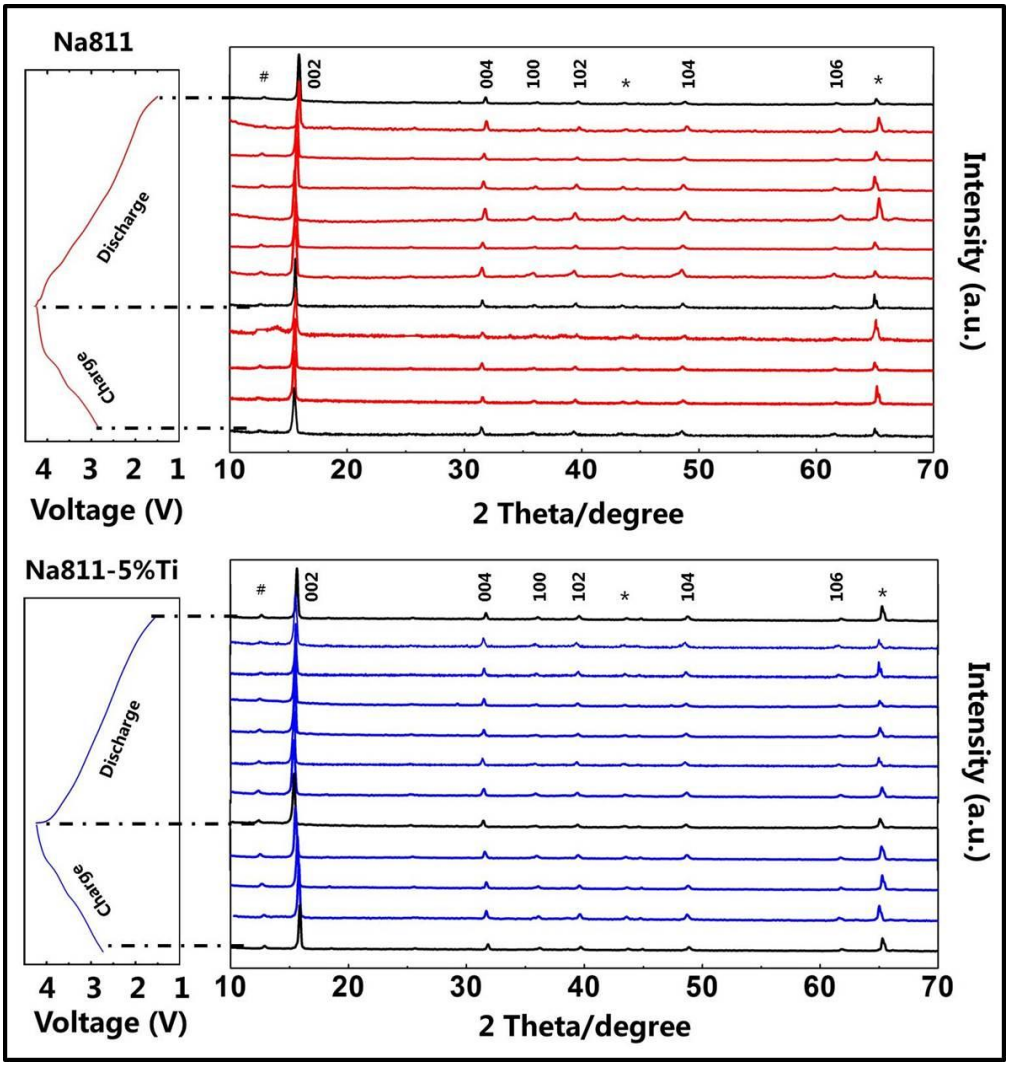

Fig. S2. *In-situ* XRD characterization of Na811 & Na811-5%Ti.

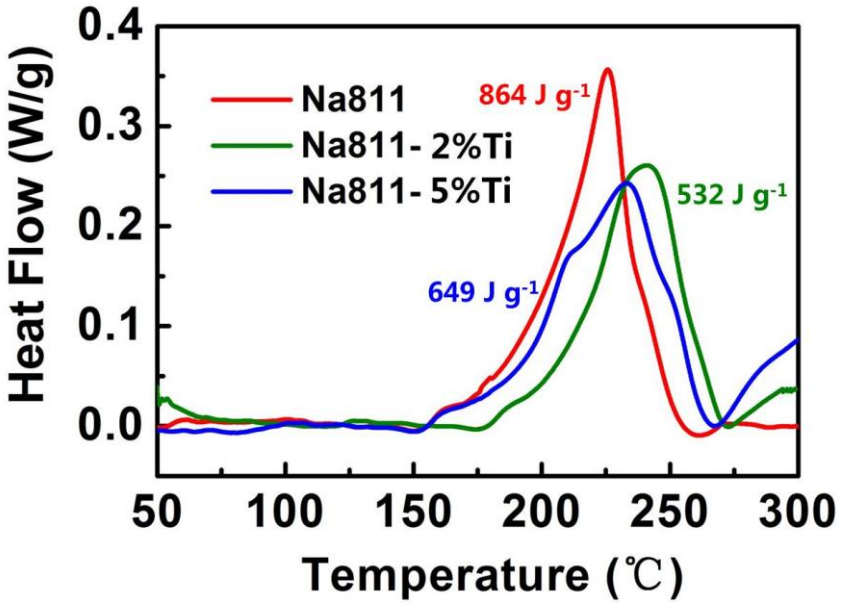

Fig. S3. DSC of Na811, Na811-2%Ti, Na811-5%Ti.

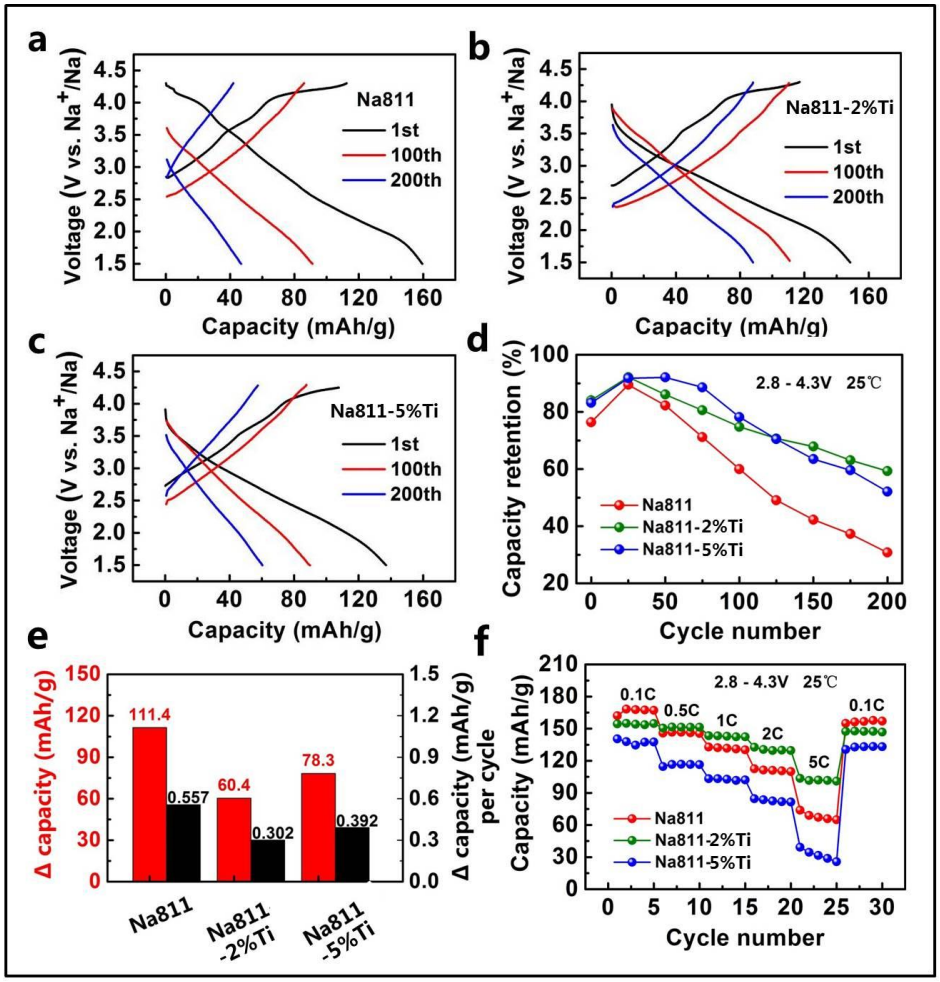

Fig. S4. Charge and discharge profiles at selected cycles at 0.1C (1st) and 0.5C (100th & 200th): a) Na811, b) Na811-2%Ti, c) Na811-5%Ti; All samples: d) capacity retention, d) Δ capacity & Δ capacity per cycle during cycling, f) rate performance.

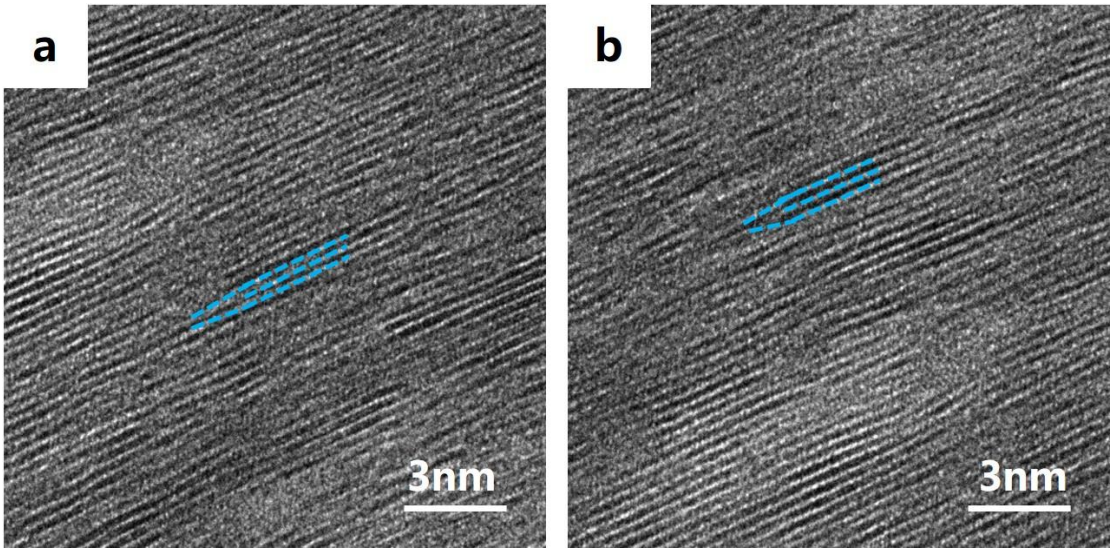

Fig. S5. The dislocation for Na811 and Na811-5%Ti after 100 charge/discharge cycles, measured

at the current rate of 0.5C.

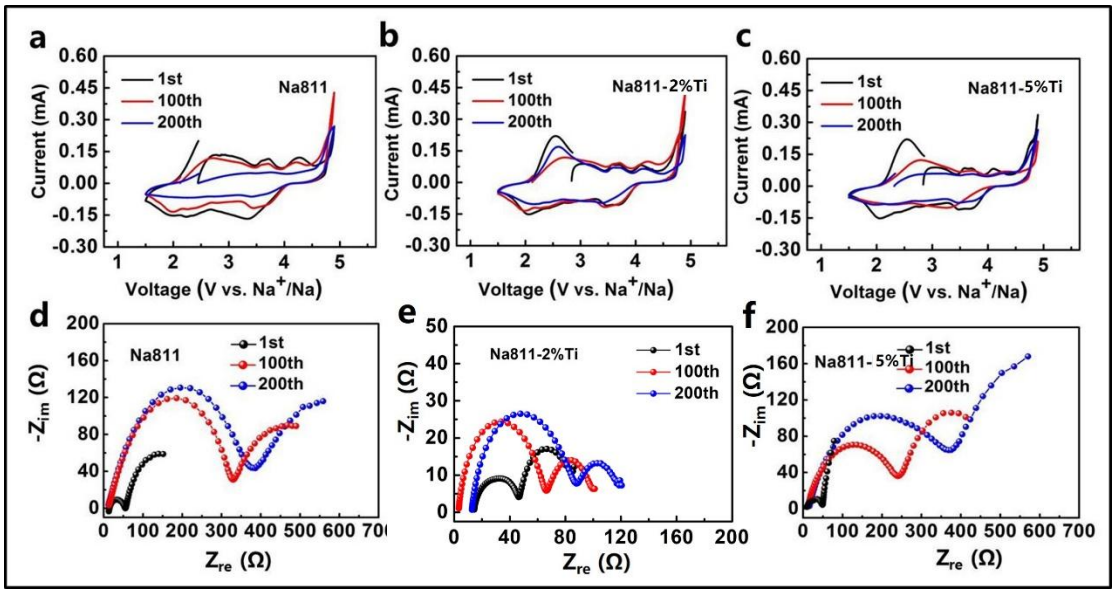

Fig. S6. Cyclic volitammograms (at scanning rate of 0.1 mV s^{-1}) and EIS spectra of 1st, 100th & 200th for the samples: a, d) Na811, b,e) Na811-2%Ti, c, f) Na811-5%Ti.

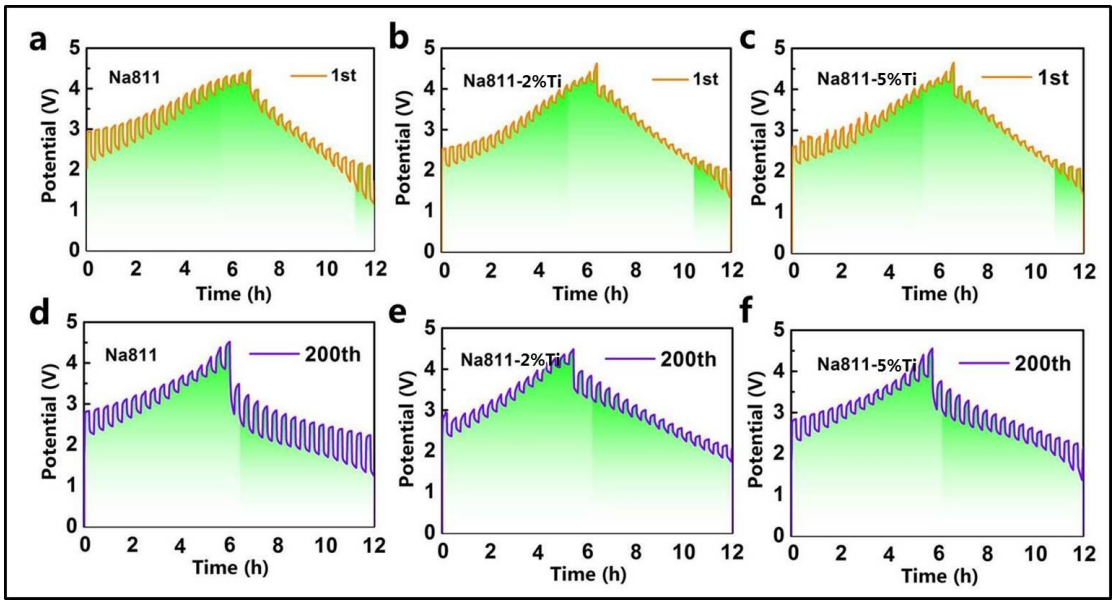

Fig. S7. The GITT of 1st and 200th for the samples: a, d) Na811, b, e) Na811-2%Ti, c, f) Na811-5%Ti.

Table S1. Crystallographic parameters of synthesized P2-$Na_{0.67}Ni_{0.1}Co0.1Mn_{0.8}O_2$ (Na811) refined by the Rietveld method.

Space group	**P63/mmc [194]**				
Atom	**site**	**X**	**Y**	**Z**	**Occ.**
Na_f	2b	0	0	0.25	0.2436
Na_e	2d	0.3333	0.6667	0.25	0.4264
Ni	2a	0	0	0	0.1000
Co	2a	0	0	0	0.1000
Mn	2a	0	0	0	0.8000
O	4f	0.6667	0.3333	0.0855	1.0000
a=2.87285 Å	c=11.28654 Å	V=80.7553Å^3	Rp=1.97%	Rwp=4.17%	

Table S2. Crystallographic parameters of synthesized P2-$Na_{0.67}Ni_{0.08}Co0.1Mn_{0.8}Ti_{0.02}O_2$ (Na811-2%Ti) refined by the Rietveld method.

Space group	**P63/mmc [194]**				
Atom	**site**	**X**	**Y**	**Z**	**Occ.**
Na_f	2b	0	0	0.25	0.2488
Na_e	2d	0.3333	0.6667	0.25	0.4212
Ni	2a	0	0	0	0.0783
Co	2a	0	0	0	0.1026
Mn	2a	0	0	0	0.7991
Ti	2a	0	0	0	0.0200
O	4f	0.6667	0.3333	0.0733	1.0000
a=2.88061 Å	c=11.28716 Å	V=81.4129Å^3	Rp=1.61%	Rwp=4.06%	

Table S3. Crystallographic parameters of synthesized P2-$Na_{0.67}Ni_{0.05}Co0.1Mn_{0.8}Ti_{0.05}O_2$ (Na811-5%Ti) refined by the Rietveld method.

Space group	**P63/mmc [194]**				
Atom	**site**	**X**	**Y**	**Z**	**Occ.**
Na_f	2b	0	0	0.25	0.2246
Na_e	2d	0.3333	0.6667	0.25	0.4454
Ni	2a	0	0	0	0.0507
Co	2a	0	0	0	0.0999
Mn	2a	0	0	0	0.7994
Ti	2a	0	0	0	0.0500
O	4f	0.6667	0.3333	0.0733	1.0000

a=2.88150 Å	c=11.28938 Å	V=81.8762Å^3	Rp=1.89%	Rwp=4.12%